



A plasmonic fiber optic absorbance biosensor for mannose-capped lipoarabinomannan based tuberculosis diagnosis

Divagar M^{a,b}, Ramakrishna Bandaru^{b,c}, Vani Janakiraman^{a,**}, V.V.R. Sai^{b,*}

^a Department of Biotechnology, Indian Institute of Technology Madras, Chennai, 600036, India

^b Biomedical Engineering Division, Department of Applied Mechanics, Indian Institute of Technology Madras, Chennai, 600036, India

^c Current Affiliation: SRM Institute of Science and Technology, Tankular, Chennai, 603203, India

ARTICLE INFO

Keywords:

Tuberculosis
Plasmonic fiber-optic absorbance biosensor
Mannosylated lipoarabinomannan
Sandwich immunoassay
Attomolar analyte detection

ABSTRACT

Tuberculosis (TB) is a resurgent infectious disease affecting a large number of people in the developing countries. An on-site, affordable diagnostic screening at an early-stage for an immediate anti-TB treatment is known to tremendously minimize the high mortality rates. Lipoarabinomannan (LAM), a surface glycolipid, has been identified as a potential TB biomarker present in urine at ultra-low concentrations of a few fg/mL. Here, we report a plasmonic fiber optic absorbance biosensor (P-FAB) strategy for mannosylated LAM (Man-LAM or *Mtb* LAM) detection down to attomolar concentrations. It involves a plasmonic sandwich immunoassay on a U-bent fiber optic probe with gold plasmonic (AuNP) labels functionalized with anti-*Mtb* LAM immunoglobulin M (IgM) and anti-*Mtb* LAM IgG respectively. The *Mtb* LAM is quantified in terms of absorption of light passing through the fiber probe using a green LED and a photodetector. The choice of fiber optic probes (fused silica versus polymer), the optimum size (20, 40, 60 and 80 nm) and concentration ($2 \times$, $10 \times$, and $20 \times$) of AuNP labels were investigated to obtain high sensitivity and lower limits of analyte detection (LoD). P-FAB with a simple LED-photodetector pair, 200 μ m fused silica U-bent fiber probe and 60 nm ($20 \times$) AuNP labels gave LoDs down to 1 fg/mL and 10 fg/mL in the buffer and synthetic urine respectively. Moreover, the anti-*Mtb* LAM IgM bound sensor probes and the AuNP reagent stored at 4 °C were stable up to 45 days. P-FAB based *Mtb* LAM sensor demonstrates its potential for an on-site TB diagnosis.

1. Introduction

Tuberculosis (TB), a chronic disease caused by the bacteria *Mycobacterium tuberculosis* (*Mtb*), re-emerged over past two decades as a major global health challenge mainly because several developing countries including India suffer from a high burden of TB, multi-drug resistant TB and HIV-TB co-infection (Daley, 2019; Macneil et al., 2019; World Health Organisation, 2019). The high mortality rate in the case of TB infection is mainly due to the delayed diagnosis that, in turn leads to the severity of the disease resulting in the chronic disability of lungs. This further intensifies the chance of disease transmission, and also healthcare expenditure (Dhedda et al., 2013). Early diagnosis and the start of timely anti-TB treatment have been shown to reduce the mortality rate significantly and spreading of infection (Holtz et al., 2011). Presently practiced standard TB diagnostic tests rely on detecting *Mtb* through the culture of sputum samples or sputum smear microscopy

(Parry et al., 1995; Habeenzu et al., 1998; Caviedes et al., 2000; Cho and Brennan, 2007) are limited by very long turn-around time (2–3 weeks) and requirement of sophisticated biosafety level 3 (BSL3) laboratories (Hamasur et al., 2001). While the Xpert MTB/RIF, a nucleic acid amplification test (NAAT), recommended by WHO allows a rapid and accurate diagnosis for patients with symptoms of TB. Although, the capital requirement for the equipment and subsidy on each test has limited its reach in resource-poor developing countries such as India. On the other hand, these techniques are not suitable for the diagnosis of extrapulmonary TB cases and in pediatric patients where sputum aspiration is difficult.

As an alternative to the above-mentioned techniques, the presence of several *Mtb* antigens in the serum, urine, or other bodily fluids has been widely investigated to establish them as potential biomarkers (Druszczyńska et al., 2017; Gopinath and Singh, 2009; Steingart et al., 2011). In the recent past, lipoarabinomannan (LAM), a glycolipid of 17–18 kDa

* Corresponding author.

** Corresponding author.

E-mail addresses: vani@iitm.ac.in (V. Janakiraman), vvr sai@iitm.ac.in (V.V.R. Sai).

<https://doi.org/10.1016/j.bios.2020.112488>

Received 18 May 2020; Received in revised form 16 July 2020; Accepted 30 July 2020

Available online 31 July 2020

0956-5663/© 2020 Elsevier B.V. All rights reserved.

and an integral component of the cell wall and cell membrane of *Mtb* and accounting for about 15% of the total bacterial dry weight, has been widely explored as a biomarker for TB diagnosis (Hamasur et al., 2001). It is known that LAM is released into the blood stream during an active TB infection, and is assumed to be cleared through kidneys and thus appears in the urine in an antigenically intact form, irrespective of the anatomical location of the infection (Hamasur et al., 2001). Several recent studies show a strong evidence for the presence of LAM up to a few ng/mL in pre-concentrated urine samples of patients with active TB without HIV co-infection and/or renal tract infections (Amin et al., 2018; Bulterys et al., 2019; Paris et al., 2017). Thus, urinary LAM could be a potential biomarker for not only pulmonary TB but also certain non-conventional TB cases such as pulmonary TB with insufficient sputum sample for analysis especially in children and extrapulmonary TB that otherwise involves laborious and complex invasive biopsy procedures for disease confirmation (Lawn and Gupta-Wright, 2015). In addition to these advantages, urinary LAM based TB detection has further merits such as ease in sample collection, handling and disposal, low protein/interferent background, and no infection risks, unlike in the case of blood or sputum for diagnosis.

Towards realizing a point-of-care (PoC) LAM test, firstly lateral flow assay (LFA) based TB LAM test kits have been developed and commercialized. However they are particularly suitable for HIV positive patients to detect TB co-infection, taking advantage of the abundance of LAM

above ng/mL concentrations (Broger et al., 2019; Hamasur et al., 2015; Reither et al., 2009; Wood and Lawn, 2012). Since the *Mtb* LAM concentrations are typically below pg/mL in unprocessed urine samples for an active TB infection, several efforts are under way to develop highly sensitive detection techniques. Some of them include LFA based Fujifilm SILVAMP and research consortia under FIND (Broger et al., 2019), single molecule fluorescence assay (FLISA) to detect urinary LAM in clinical samples of HIV negative patients at ultra-low concentration of fg/ml (Wood et al., 2019). Recently, our research group has developed a plasmonic fibreoptic absorbance biosensor (P-FAB) strategy with analyte detection limits down to 1 fg/mL of immunoglobulin G (IgG). It involves the realization of a sandwich immunoassay with gold nanoparticles (AuNP) labels on a U-bent fiber optic sensor using a pair of LED and photodetector, as shown in Fig. 1 (Ramakrishna et al., 2020; Ramakrishna and Sai, 2016). The high sensitivity and ultra-low analyte detection limits of the P-FAB arise from the improved evanescent field of the optimal U-bend geometry, leading to a high evanescent wave absorbance (EWA) sensitivity (Danny et al., 2020). The EWA of the U-bent sensor probes due to the presence of a small number of AuNP, but with a large optical extinction coefficient ($\sim 10^{10} \text{ M}^{-1}\cdot\text{cm}^{-1}$), on its surface gives rise to a measurable drop in the intensity of light passing through the probe.

Here, we exploit the wash-free plasmonic fiber optic absorbance biosensor (P-FAB) strategy for the detection of mannoseylated

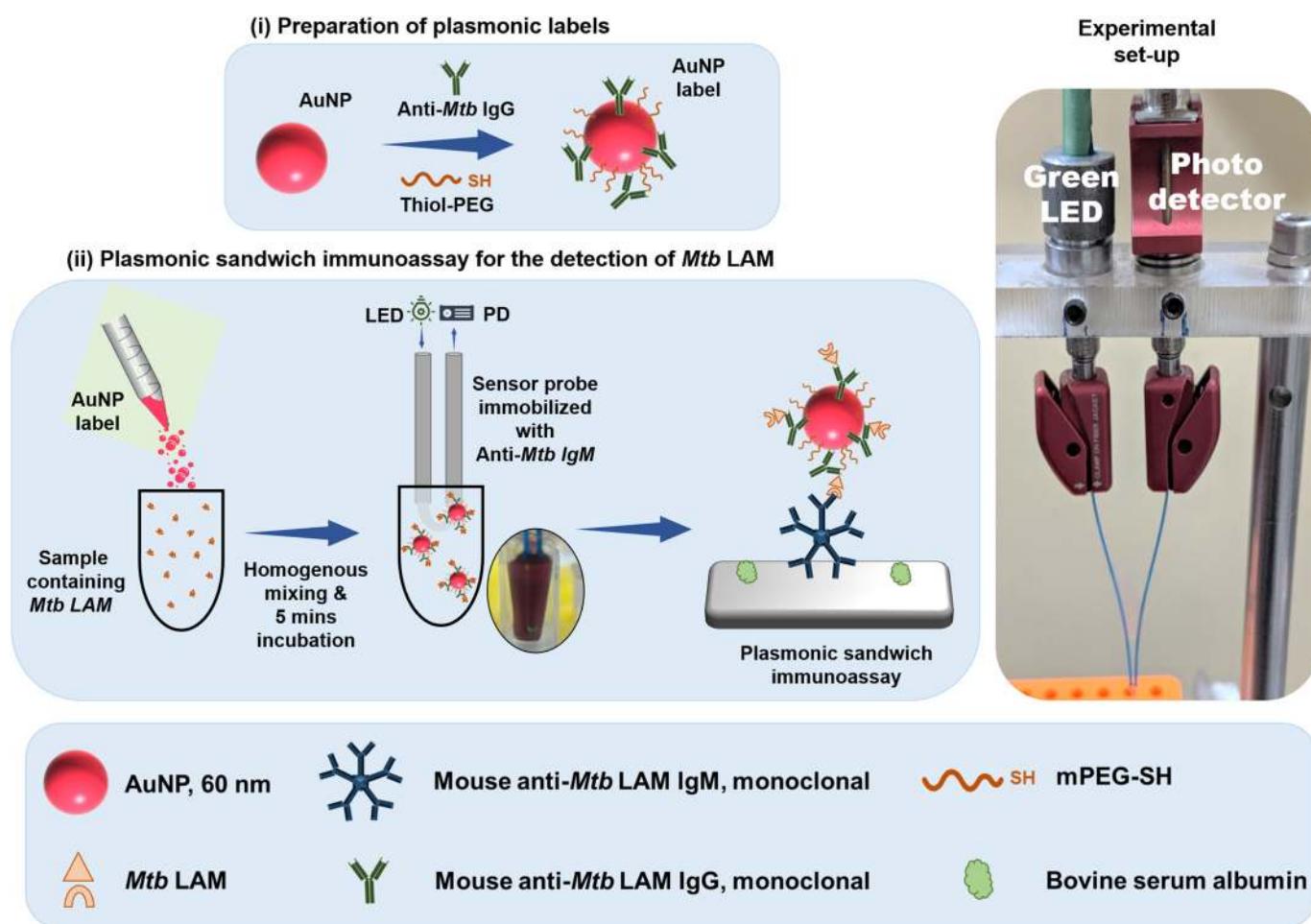


Fig. 1. Schematic representation of plasmonic sandwich immunoassay for the detection of *Mtb* LAM in the urine samples of TB patients. The photographic image of the experimental set-up shows a U-bent fiber optic probe connected between a pair of LED and a photodetector using bare fiber adaptors. A green LED (525 nm) was chosen to match with the plasmonic absorbance peak of the AuNP conjugates. The drop in the light intensity at the PD due to the evanescent wave absorption as a result of the plasmonic sandwich immunocomplex was plotted as an absorbance (referred as sensor response) by taking the logarithm ratio of the initial (I_0) to final power intensity (I_t) values to highlight smaller changes for low analyte concentrations. (For interpretation of the references to colour in this figure legend, the reader is referred to the Web version of this article.)

lipoarabinomannan (Man-LAM, also referred to as *Mtb* LAM) in a buffer as well as in a synthetic urine. In the process of realizing a P-FAB for *Mtb* LAM detection, the optimum size and concentration of the plasmonic labels and a comparison of fused silica and polymeric optical fiber based U-bent probes were investigated to obtain ultrasensitive sensor performance using model analytes (human IgG). Later, a plasmonic sandwich immunoassay was realized using anti-*Mtb* LAM immunoglobulin M (IgM) as a capture antibody immobilized on the U-bent fiber optic probe and anti-*Mtb* LAM IgG specific to another epitope on *Mtb* LAM as a detector antibody conjugated AuNP labels (Fig. 1). The plasmonic sandwich immunocomplex that formed on the U-bent sensor probe surface in the presence of *Mtb* LAM is quantified as optical power loss in the U-bent probe using a simple LED and photodetector pair. The optical power losses due to AuNP labels are quantified for various concentrations of *Mtb* LAM between 1 fg/mL and 1 ng/mL using a simple green LED and photodetector pair. In addition, the shelf-life of the antibody-coated sensor probe and the AuNP reagent was assessed over a duration of 60 days.

2. Results and discussion

2.1. Optimization of AuNP label size and concentration for P-FAB

The high sensitivity of the P-FAB based sensing strategy originates from the unique ability of the U-bent optical fiber probes to detect the plasmonic AuNP labels with a large optical extinction coefficient binding to the bend region. The optical extinction property of these AuNP labels, which enables the ultra-low analyte detection limits, is highly dependent on their size, as shown in Fig. S1. Moreover, the concentration of the AuNP conjugated with detector antibodies is another critical factor that determines the availability of a sufficient number AuNP bioconjugates for efficient capture of analytes, and the mobility/kinetics of the immunocomplex in the solution phase.

In order to investigate the optimum AuNP size, P-FAB based sandwich immunoassay was realized with 20, 40, 60, and 80 nm AuNP labels (Fig. S2A). The optical density of the AuNPs (BBI solutions, UK) at their peak wavelength equal to unity was taken as a reference to compare the influence of AuNP label size Table S1. (It may be noted that comparison of AuNP sizes can be highly complex for a sandwich immunoassay given many other influential parameters including the number density of AuNP, the number of antibodies conjugated to each nanoparticle, and

their interaction with analytes in the solution phase). The experiments were realized on 500 μm polymeric optical fiber (POF) based U-bent sensor probes (Gowri and Sai, 2016) with a set-up, as shown in Fig. S2B. The green LED (peak at 525 nm) used in the set-up has a suitable optical intensity profile to efficiently excite all the label sizes (at least 73% for 80 nm labels) (Table S2). The sandwich immunoassay was realized with human IgG (HIgG) as a model analyte and goat anti-HIgG antibodies specific to F_{ab} and F_c regions of HIgG as described elsewhere (Fig. S2B) (Divagar and Sai, 2018).

Fig. 2 shows the sensor response obtained with the AuNP label sizes over a range of HIgG concentrations from 0 to 1000 ng/mL. AuNP labels of 60 nm gave rise to a consistently higher P-FAB response for all the HIgG concentrations in comparison to the other sizes (Fig. S3). Unlike the increasing trend in the extinction coefficient for AuNP size, the P-FAB sensitivity was found to improve by 4-folds up to 60 nm AuNP labels followed by an abrupt drop in the case of 80 nm. (Fig. S4). The SEM images of the probes show a noteworthy reduction in the surface density of AuNP labels with the increase in AuNP label size (Fig. S3D). Despite the higher surface density, 20 and 40 nm AuNP labels show a lower sensor response in comparison to 60 nm AuNP labels, mostly due to their lower extinction coefficients. On the other hand, we anticipate steric hindrance effects in binding of the analyte-AuNP complex to the sensor surface (Springer et al., 2014; Wu et al., 2018). The observed trend in the sensor response corroborates well with the theoretical estimate of optical extinction obtained based on the extinction cross-sectional area and the observed number density of the AuNPs for each size (Table S3). Thus 60 nm AuNP labels are found to be optimum for P-FAB.

Further, the effect of AuNP label concentration on the sensor response was studied using the optimized AuNP labels of 60 nm in size. AuNP label concentrations of 2 \times , 10 \times and 20 \times were analysed using 1 $\mu\text{g}/\text{ml}$ of HIgG as an analyte. The results show two-fold improvement in the sensor response with 20 \times concentration, however, with a rise in the standard deviation of over 10% (Fig. 2B). This could be attributed to the enhanced availability of the number of AuNP labels within the vicinity of the biofunctionalized fiber core surface (Shahriari et al., 2016). The subsequent dose response studies carried out with 20 \times concentration indeed show an improved detection analyte detection limits down to 100 fg/ml (Fig. S5).

In addition to the AuNP labels, the choice of U-bent probe is the other critical aspect of P-FAB. Here, the sensitivity of the fused silica (200 μm core) and polymeric (500 μm) optical fiber (GOF and POF respectively)

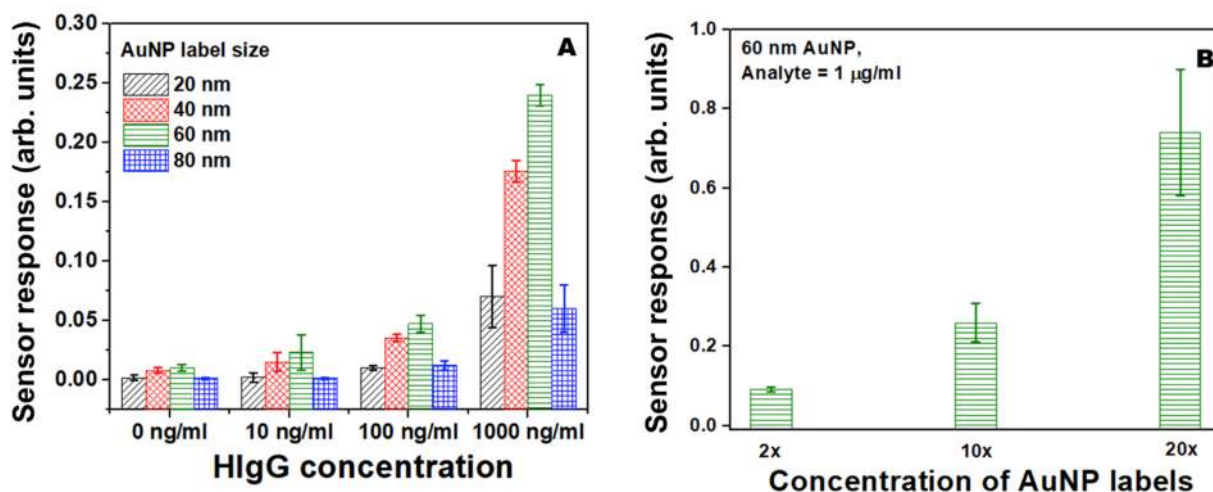


Fig. 2. Optimization of AuNP label size and concentration for P-FAB. (A) P-FAB response obtained using the U-bent POF sensor probe and different sizes of AuNP labels (10 \times , meaning the optical density of bare AuNP at its peak wavelength was 10 arb units) from 20 to 80 nm for various concentrations of HIgG as analyte. The protocol shown in Fig. S2B was followed, and the sensor response was recorded over 20 min and compared. (B) Influence of AuNP 60 nm label concentration on the P-FAB response for 1 $\mu\text{g}/\text{mL}$ of HIgG.

based U-bent probes was evaluated by comparing their dose response for HIgG as an analyte. An improved sensor response was observed in the case of GOF over the POF (Fig. S6). We anticipate an increase in the number density of sandwich immunocomplexes per unit surface area for a 200 μm fiber and hence a higher optical absorbance for a given analyte as responsible for the improved sensor performance (Danny et al., 2020; Ramakrishna et al., 2020). However, several other factors, including the probe surface biofunctionalization efficacy and evanescent field at the core-cladding interface, may also contribute to the observed phenomenon, each of which requires a detailed investigation and outside the scope of this work. Based on the above results, all the subsequent studies were carried out with 200 μm core GOF U-bent probes and 60 nm AuNP labels at 20 \times concentration.

2.2. Realization of P-FAB strategy for *Mtb* LAM detection

To establish a proof-of.-concept for P-FAB based *Mtb* LAM detection, the fused silica U-bent probe and 60 nm AuNP were biofunctionalized with IgM and IgG against *Mtb* LAM respectively. Since the ligand-analyte pair in this study involves IgM and *Mtb* LAM, a pentameric form of the routinely used IgG and a glycolipid respectively, the optimum conditions for bioreceptor (IgM) immobilization over U-bent GOF probe surface were investigated as the first step towards the realization of P-FAB based *Mtb* LAM detection. The fiber probe surface modification and anti-*Mtb* LAM IgM immobilization are illustrated in Fig. S7a. The silica core surface was modified with amino-silane followed by glutaraldehyde to obtain amine (-NH₂) and aldehyde (-CHO) functional groups, respectively. Subsequently, the presence of -NH₂ and -CHO functional groups was verified by using fluorescein isothiocyanate (FITC, 1 mM) and 2,4 dinitrophenyl hydrazine (2,4 DNPH), respectively. The surface modification was confirmed by the evanescent wave (EW) based absorbance spectral response shown in Figs. S7B and C. Subsequently, the studies to investigate an optimum anti-*Mtb* LAM IgM concentration for immobilization suggest a saturated surface coverage at 50 $\mu\text{g}/\text{mL}$ (Fig. S7D).

On the other hand, the conjugation of monoclonal anti-*Mtb* LAM IgG antibodies to AuNPs was confirmed from optical absorbance spectra (USB4000, Ocean Optics) and dynamic light scattering measurements. A red-shift of 3 nm in LSPR spectral peak was observed due to RI changes caused by IgG binding to the AuNP (Fig. S8). DLS measurements too showed an increase in their mean effective diameter from 60.3 \pm 0.3 nm to 83.3 \pm 1.4 nm ($n = 3$) similar to other reports, confirming the IgG conjugation to 60 nm AuNP. The significant increase in the effective diameter suggests conjugation of most of the antibodies to AuNP surface in their head-on or end-on position. Still, an increase in the polydispersity index from 0.136 \pm 0.007 to 0.221 \pm 0.009 ($n = 3$) also indicates the immobilization of a small fraction of antibodies in the other side-on and flat orientations (Tripathi and Driskell, 2018).

Subsequent to establishing the biofunctionalization of GOF U-bent probes and bioconjugation of 60 nm AuNP, a sandwich immunoassay was realized by using a set-up consisting of a broadband green LED and fiber optic spectrometer (Fig. S9A) and following a protocol shown in Fig. 1. Optical absorbance spectra were recorded during the formation of plasmonic immunocomplex formation on the probe surface (Fig. S9B). The peak absorbance was found to be \sim 540 nm for AuNP 60 nm. The fiber optic spectrometer based set-up was able to distinguish *Mtb* LAM concentrations between 1 and 100 ng/mL (Fig. S9C).

2.3. P-FAB based *Mtb* LAM detection – dose response

The P-FAB response to *Mtb* LAM concentrations of interest between 1 fg/mL (59 aM) and 100 pg/mL (6 pM) (containing 10⁴ to 10⁹ *Mtb* LAM molecules) in PBS buffer was evaluated to determine the sensitivity and, the analyte detection limit. The saturated response was obtained for each analyte concentration ($n = 5$), as shown in Fig. 3A. Similarly, the sensor responses were obtained for *Mtb* LAM spiked synthetic urine

(Fig. 3B). The SEM images of AuNP labels were obtained from the U-bent probes after the assay. The SEM images (Fig. 3C) clearly show a distinguishable surface density of the plasmonic complex over the probe surface for the various concentrations of *Mtb* LAM. Dose response curves for *Mtb* LAM prepared in PBS buffer, and synthetic urine were plotted based on the sensor response at the end of 3000 s, as shown in Fig. 3D. A linear response was obtained over the range of analyte concentration tested in this study. The sensor characteristics, including the sensitivity, limit of detection (LoD), and measurement range given in Table 1 were calculated as follows. The sensitivity was obtained from the slope of the linear fit applied to the dose response curves such that the positive Pearson's value for the chosen analyte concentration range is close to unity (0.99). The slower binding kinetics and \sim 50% reduction in the sensitivity for *Mtb* LAM detection in synthetic urine in comparison to PBS could be attributed to (i) the smaller diffusion coefficient for AuNP-IgG-LAM complex caused by the presence of a high concentration of the interfering biomolecules (BSA and creatinine) (Giorgi et al., 2019), (ii) higher protein concentration could also interfere with the binding of AuNP-IgG-LAM complex with the IgM immobilized on the sensor probe, the influence could be seen as a marginal increase in the sensor response at 0 fg/mL in synthetic urine as compared with PBS, and (iii) its pH (\sim 6.5) leading to a drop in the affinity of the antibodies towards the analyte (Yalov et al., 1975).

The limit of detection (LoD) estimates of the sensor probe as per the conventional method of $3\sigma/S$ give rise to 0.26 fg/mL and 0.3 fg/mL for LAM in PBS and synthetic urine, respectively. However, as per the guideline EP17 provided by Clinical and Laboratory Standards Institute (CLSI) (Armbruster and Pry, 2008), where $\text{LoD} = \text{LoB} + 1.645(\text{SD}_{\text{low-concentration sample}})$, and LoB is the limit of blank ($\text{LoB} = \text{mean}_{\text{blank}} + 1.645(\text{SD}_{\text{blank}})$), an LoD of 1 fg/mL LAM in PBS was obtained. Although the LoD worsen to 10 fg/mL in the case of synthetic urine, it is anticipated to be sufficient and relevant for the LAM detection in urine for TB diagnosis (Wood et al., 2019). A comparison of these results with various other biosensing schemes reported in the literature shows that P-FAB strategy is very promising for LAM detection (Table S4).

2.4. P-FAB based *Mtb* LAM detection – shelf-life studies

A successful realization of P-FAB *Mtb* LAM sensor towards pre-clinical studies and subsequent technology demonstration demands a stable and reliable sensor response, which is highly influenced by the shelf-life of the two consumables involved in the assay, namely the IgM functionalized U-bent probes and the IgG conjugated AuNP label reagent. The shelf-life studies were carried out with anti-*Mtb* LAM IgM functionalized U-bent probes ($n = 50$) kept in nitrogen ambience and AuNP reagent were stored at 4 $^{\circ}\text{C}$. Their activity was monitored every 15 days (up to 60 days) by obtaining the sensor response for *Mtb* LAM of 0 fg/ml ($n = 3$) and 10 fg/ml ($n = 3$) spiked in PBS buffers solutions. The experiments for evaluation of the shelf-life of stored probes and the reagent were carried out with the freshly prepared reagent and probes, respectively. As a reference (referred as C in Fig. 4), their sensor response was compared against that of freshly prepared bio-functionalized U-bent probes and AuNP label reagent for each run. Fig. 4A shows P-FAB *Mtb* LAM sensor response with stored U-bent probes. With reference to the control response (referred to as C - 10 fg/mL), the stored probe response (referred to as P - 10 fg/mL) deteriorated only by 60th day, while there was no significant rise in the NSA due to the possible denaturation of IgM over the probe surface (P - 0 fg/mL) with respect to the control (C - 0 fg/mL). Fig. 4B shows P-FAB *Mtb* LAM sensor response with stored AuNP reagent (R - 10 fg/mL), which showed a marginal deviation from the reference response (C - 10 fg/mL) after 15th day and a significant drop (up to 12% decrement) beyond 45th day. In addition, a considerable rise in the non-specific adsorption (R - 0 fg/mL) was observed by the 60th day, which could be attributed to the degradation of IgG on the AuNP surface, leading to increased chemisorption to the probe surface. Hence, it may be concluded that the sensor

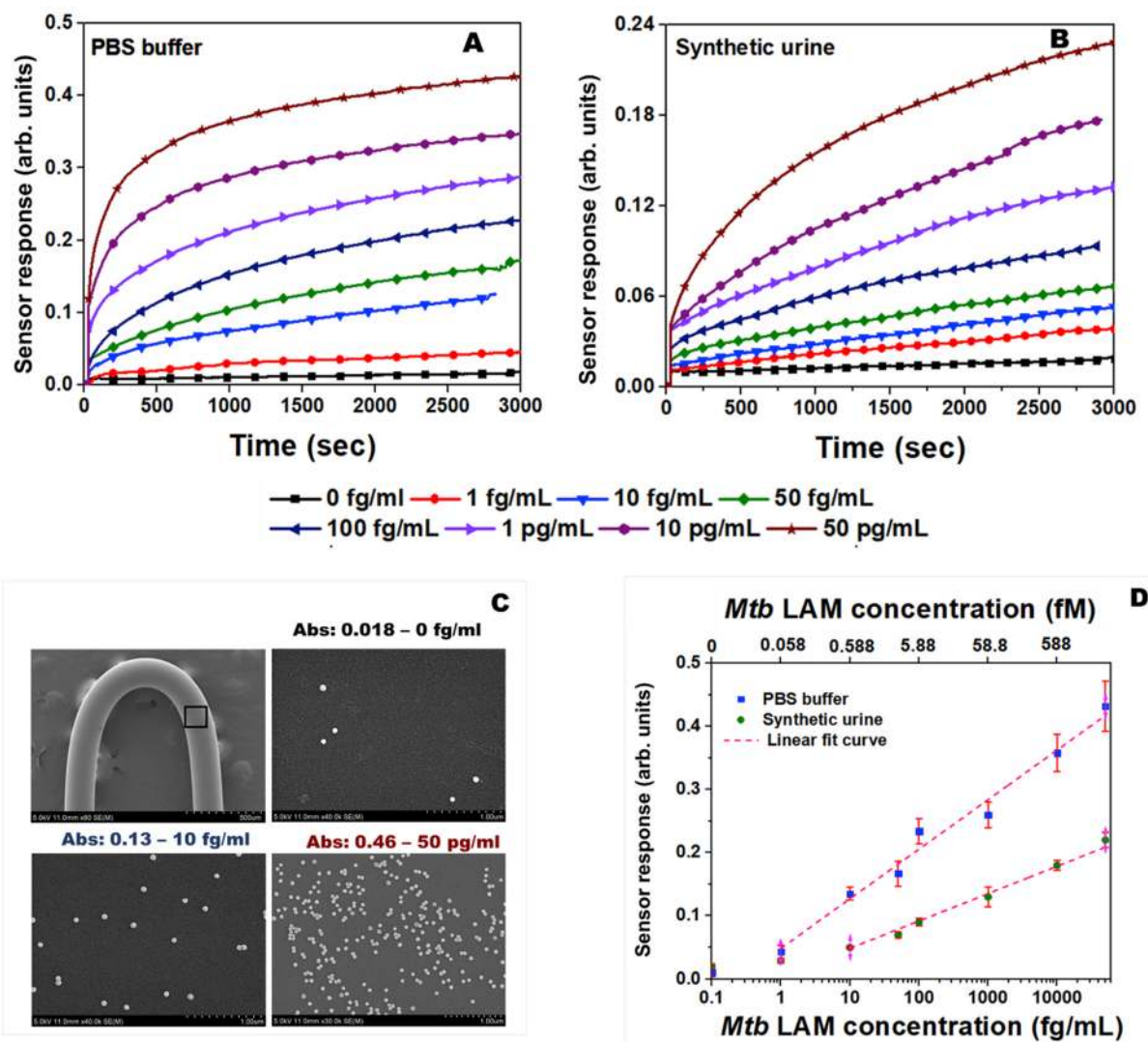


Fig. 3. Top row: Temporal responses showing an increase in the optical absorbance due to the formation of plasmonic sandwich immunocomplexes on the sensor probe surface for different concentrations of *Mtb*. LAM in (A) PBS and (B) synthetic urine. Bottom row: (C) SEM images of the sensor probes subjected to different concentrations of LAM analyte showing an increase in AuNP density with LAM concentration. (D) The P-FAB dose-response curves obtained with PBS buffer and synthetic urine spiked with the known concentration of *Mtb* LAM.

Table 1
P-FAB *Mtb* LAM sensor characteristics for LAM in PBS and synthetic urine.

P-FAB LAM sensor matr	LAM in PBS	LAM in synthetic urine
Sensitivity ($A_{542 \text{ nm}}/\log(\text{fg/mL})$) ($R^2 = 0.98$)	0.078	0.043
LoD (fg/mL, (aM))	1 (59)	10 (590)
Dynamic range	5 fg/ml to 10 pg/mL	10 fg/ml to 10 pg/mL

probes have a shelf-life of about 45 days, while the AuNP label reagent undergoes a significant degradation beyond 45 days. We anticipate a better stability and shelf-life by vacuum-sealing of the probes and a solid-phase storage of AuNP reagent as in the case of lateral flow assays (Sajid and Daud, 2015) for example, water-dissolvable paper strips that readily dissolve after coming in contact with the sample.

3. Conclusion

A plasmonic fiber optic biosensor (P-FAB) strategy is optimized with

respect to the AuNP label size and concentration and type of optical fiber for the U-bent sensor probe to obtain the maximum possible sensitivity. Under the conditions investigated in this study, AuNP label size of 60 nm at $20 \times$ concentration and fused silica fiber of 200 μm core diameter were found to be optimum. A P-FAB for *Mtb* LAM detection is established with a minimum detection limit of 1 fg/mL (59 aM) and 10 fg/mL (0.59 fM) for *Mtb* LAM spiked in the PBS buffer as well as synthetic urine samples respectively. Our preliminary studies show a better diffusion and sensitivity with real urine samples. Further studies are in progress to evaluate the sensor performance for real samples. These results demonstrate that the P-FAB is highly promising for an equipment-free, affordable, on-site TB diagnosis owing to its advantages, including a simple LED-PD based optoelectronic instrumentation with a plausible easy detachable optical coupling of U-bent probes, one-step wash-free sandwich assay, and stable biofunctionalized U-bent probes and AuNP reagent.

CRedit authorship contribution statement

Divagar M: Conceptualization, Methodology, Investigation, Writing - original draft. **Ramakrishna Bandaru:** Methodology. **Vani**

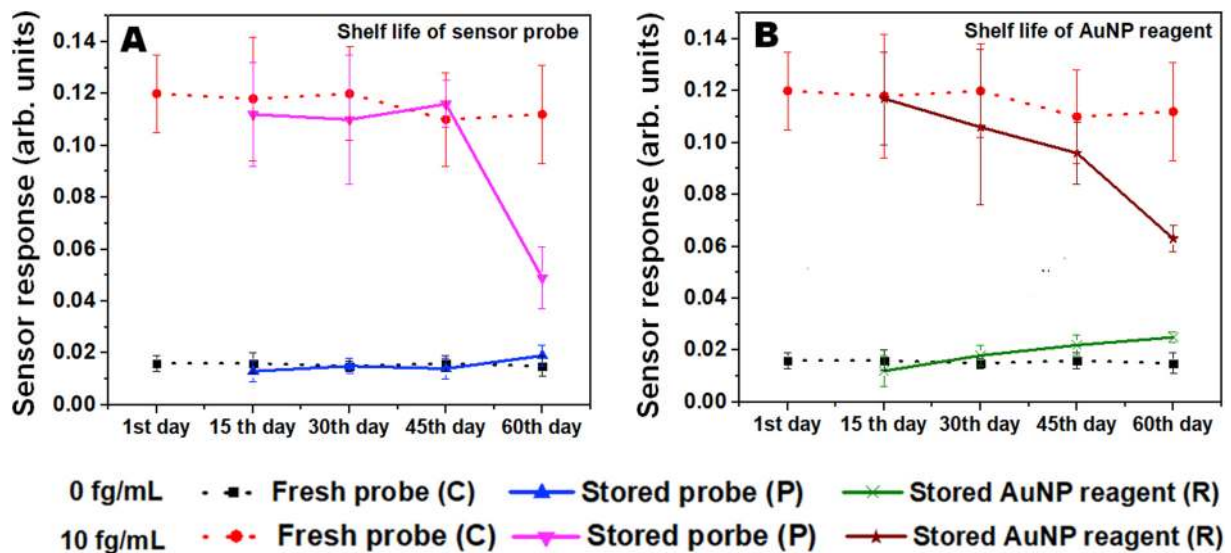


Fig. 4. P-FAB response illustrating the shelf-life of the (A) antibody immobilized sensor probes and (B) AuNP labels stored at 4 °C and assessed every 15 days over a duration of 60 days. C refers to the overall control experiment with a freshly biofunctionalized U-bent sensor probe and the plasmonic reagent as a reference. P refers to experiments with stored sensor probes using freshly prepared AuNP reagent, and R refers to experiments on freshly prepared sensor probes using the stored AuNP reagent.

Janakiraman: Conceptualization, Writing - original draft, Supervision.
V.V.R. Sai: Conceptualization, Writing - original draft, Supervision.

Declaration of competing interest

The authors declare that they have no known competing financial interests or personal relationships that could have appeared to influence the work reported in this paper.

Acknowledgments

VVRS acknowledges the research grant from IIT Madras and Indo-German Science and Technology (IGSTC) for partial financial support. DM acknowledges Department of Science and Technology (DST) INSPIRE PhD Fellowship from the Government of India. We acknowledge the HR-SEM facility in the Department of Chemical Engineering, IIT Madras, funded by DST- Fund for Improvement of S&T Infrastructure in Universities and Higher Educational Institutions (DST-FIST) program from the Government of India.

Appendix A. Supplementary data

Supplementary data to this article can be found online at <https://doi.org/10.1016/j.bios.2020.112488>.

References

- Amin, A.G., De, P., Spencer, J.S., Brennan, P.J., Daum, J., Andre, B.G., Joe, M., Bai, Y., Laurentius, L., Porter, M.D., William, J., Choudhary, A., Lowary, T.L., Pinter, A., Chatterjee, D., 2018. Detection of lipoarabinomannan in urine and serum of HIV-positive and HIV-negative TB suspects using an improved capture-enzyme linked immuno absorbent assay and gas chromatography/mass spectrometry. *Tuberculosis* 111, 178–187. <https://doi.org/10.1016/j.tube.2018.06.004>.
- Armbruster, D.A., Pry, T., 2008. Limit of blank, limit of detection and limit of quantitation. *Clin. Biochem. Rev.* 29 (Suppl. 1), S49–S52.
- Broger, T., Sossen, B., du Toit, E., Kerkhoff, A.D., Schutz, C., Ivanova Reipold, E., Ward, A., Barr, D.A., Macé, A., Trollip, A., Burton, R., Ongarello, S., Pinter, A., Lowary, T.L., Boehme, C., Nicol, M.P., Meintjes, G., Denking, C.M., 2019. Novel lipoarabinomannan point-of-care tuberculosis test for people with HIV: a diagnostic accuracy study. *Lancet Infect. Dis.* 19, 852–861. [https://doi.org/10.1016/S1473-3099\(19\)30001-5](https://doi.org/10.1016/S1473-3099(19)30001-5).
- Bulterys, M.A., Wagner, B., Redard-Jacot, M., Suresh, A., Pollock, N.R., Moreau, E., Denking, C.M., Drain, P.K., Broger, T., 2019. Point-of-care urine LAM tests for

- tuberculosis diagnosis: a status update. *J. Clin. Med.* 9, 111. <https://doi.org/10.3390/jcm9010111>.
- Caviedes, L., Tien-Shun, L., Gilman, R.H., Sheen, P., Spellman, E., Lee, E.H., Berg, D.E., Montenegro-James, S., Fuentes, P., Valencia, T., Chumplitaz, R., Salas, I., Recavarren, S., Cama, R., Cabrera, L., Franchi, L.M., Ticona, E., Ticona, L., Chavez, V., Vivar, A., Rodriguez, S., Checkley, W., Black, R., Franzblau, S., Friedland, J., Evans, C., 2000. Rapid, efficient detection and drug susceptibility testing of *Mycobacterium tuberculosis* in sputum by microscopic observation of broth cultures. *J. Clin. Microbiol.* 38, 1203–1208. <https://doi.org/10.1128/jcm.38.3.1203-1208.2000>.
- Cho, S.N., Brennan, P.J., 2007. Tuberculosis: diagnostics. *Tuberculosis* 87, 14–17. <https://doi.org/10.1016/j.tube.2007.05.001>.
- Daley, C.L., 2019. The global fight against tuberculosis. *Thorac. Surg. Clin.* 29, 19–25. <https://doi.org/10.1016/j.thorsurg.2018.09.010>.
- Danny, C.G., Raj, M.D., Sai, V.V.R., 2020. Investigating the refractive index sensitivity of U-bent fiber optic sensors using ray optics. *J. Lightwave Technol.* 38, 1580–1588. <https://doi.org/10.1109/JLT.2019.2958044>.
- Dhedha, K., Ruhwald, M., Theron, G., Peter, J., Yam, W.C., 2013. Point-of-care diagnosis of tuberculosis: past, present and future. *Respirology* 18, 217–232. <https://doi.org/10.1111/resp.12022>.
- Divagar, M., Sai, V.V.R., 2018. Fiber optic plasmonic sandwich immunosensor: influence of AuNP label size and concentration. *Proceedings of IEEE Sensors. IEEE*, pp. 1–4. <https://doi.org/10.1109/ICSENS.2018.8589779>.
- Druzczynska, M., Wawrocki, S., Szewczyk, R., Rudnicka, W., 2017. Mycobacteria-derived biomarkers for tuberculosis diagnosis. *Indian J. Med. Res.* 146, 700–707. https://doi.org/10.4103/ijmr.IJMR_1441_16.
- Giorgi, F., Coglitore, D., Curran, J.M., Gilliland, D., Macko, P., Whelan, M., Worth, A., Patterson, E.A., 2019. The influence of inter-particle forces on diffusion at the nanoscale. *Sci. Rep.* 9, 1–6. <https://doi.org/10.1038/s41598-019-48754-5>.
- Gopinath, K., Singh, S., 2009. Urine as an adjunct specimen for the diagnosis of active pulmonary tuberculosis. *Int. J. Infect. Dis.* 13, 374–379. <https://doi.org/10.1016/j.ijid.2008.07.022>.
- Gowri, A., Sai, V.V.R., 2016. Development of LSPR based U-bent plastic optical fiber sensors. *Sensor. Actuator. B Chem.* 230, 536–543. <https://doi.org/10.1016/j.snb.2016.02.074>.
- Habeenzu, C., Lubasi, D., Fleming, A.F., 1998. Improved sensitivity sputum in developing of direct microscopy countries. *Trans. R. Soc. Trop. Med. Hyg.* 92, 415–416.
- Hamasur, B., Bruchfeld, J., Haile, M., Pawlowski, A., Bjorvatn, B., Källenius, G., Svenson, S.B., 2001. Rapid diagnosis of tuberculosis by detection of mycobacterial lipoarabinomannan in urine. *J. Microbiol. Methods* 45, 41–52. [https://doi.org/10.1016/S0167-7012\(01\)00239-1](https://doi.org/10.1016/S0167-7012(01)00239-1).
- Hamasur, B., Bruchfeld, J., VanHelden, P., Källenius, G., Svenson, S., 2015. A sensitive urinary lipoarabinomannan test for tuberculosis. *PLoS One* 10, 1–11. <https://doi.org/10.1371/journal.pone.0123457>.
- Holtz, T.H., Kabera, G., Mthiyane, T., Zingoni, T., Nadesan, S., Ross, D., Allen, J., Chideya, S., Sunpath, H., Rustomjee, R., 2011. Use of a WHO-recommended algorithm to reduce mortality in seriously ill patients with HIV infection and smear-negative pulmonary tuberculosis in South Africa: an observational cohort study. *Lancet Infect. Dis.* 11, 533–540. [https://doi.org/10.1016/S1473-3099\(11\)70057-3](https://doi.org/10.1016/S1473-3099(11)70057-3).
- Lawn, S.D., Gupta-Wright, A., 2015. Detection of lipoarabinomannan (LAM) in urine is indicative of disseminated TB with renal involvement in patients living with hiv and advanced immunodeficiency: evidence and implications. *Trans. R. Soc. Trop. Med. Hyg.* 110, 180–185. <https://doi.org/10.1093/trstmh/trw008>.

- Macneil, A., Glaziou, P., Sismanidis, C., Maloney, S., Floyd, K., 2019. Global epidemiology of tuberculosis and progress toward achieving global targets — 2017. *Morb. Mortal. Wkly. Rep.* 68, 263–266. <https://doi.org/10.15585/mmwr.mm6811a3>.
- Paris, L., Magni, R., Zaidi, F., Araujo, R., Saini, N., Harpole, M., Coronel, J., Kirwan, D.E., Steinberg, H., Gilman, R.H., Iii, E.F.P., Nisini, R., Luchini, A., Liotta, L., 2017. Urine lipoarabinomannan glycan in HIV-negative patients with pulmonary tuberculosis correlates with disease severity. *Sci. Transl. Med.* 9, 1–12. <https://doi.org/10.1126/scitranslmed.aal2807>.
- Parry, C.M., Kamoto, O., Harries, A.D., Wirima, J.J., Nyirenda, C.M., Nyangulu, D.S., Hart, C.A., 1995. The use of sputum induction for establishing a diagnosis in patients with suspected pulmonary tuberculosis in Malawi. *Tuber. Lung Dis.* 76, 72–76. [https://doi.org/10.1016/0962-8479\(95\)90583-9](https://doi.org/10.1016/0962-8479(95)90583-9).
- Ramakrishna, B., Divagar, M., Khanna, S., Danny, C.G., Gupta, S., Janakiraman, V., S, V. V.R., 2020. U-bent fiber optic plasmonic biosensor platform for ultrasensitive analyte detection. *Sensor. Actuator. B Chem.* 321, 1–6. <https://doi.org/10.1016/j.snb.2020.128463>.
- Ramakrishna, B., Sai, V.V.R., 2016. Evanescent wave absorbance based U-bent fiber probe for immunobiosensor with gold nanoparticle labels. *Sensor. Actuator. B Chem.* 226, 184–190. <https://doi.org/10.1016/j.snb.2015.11.107>.
- Reither, K., Saathoff, E., Jung, J., Minja, L.T., Kroidl, I., Saad, E., Huggett, J.F., Ntinginya, E.N., Maganga, L., Maboko, L., Hoelscher, M., 2009. Low sensitivity of a urine LAM-ELISA in the diagnosis of pulmonary tuberculosis. *BMC Infect. Dis.* 9, 141. <https://doi.org/10.1186/1471-2334-9-141>.
- Sajid, M., Daud, M., 2015. Designs , formats and applications of lateral flow assay : a literature review. *J. Saudi Chem. Soc.* 19, 689–705. <https://doi.org/10.1016/j.jscs.2014.09.001>.
- Shahriari, E., Moradi, M., Raeisi, M., 2016. An experimental study of thermal diffusivity of Au nanoparticles: effects of concentration particle size. *J. Theor. Appl. Phys.* 10, 259–263. <https://doi.org/10.1007/s40094-016-0224-x>.
- Špringer, T., Ermini, M.L., Špačková, B., Jablonkú, J., Homola, J., 2014. Enhancing sensitivity of surface plasmon resonance biosensors by functionalized gold nanoparticles: size matters. *Anal. Chem.* 86, 10350–10356. <https://doi.org/10.1021/ac502637u>.
- Steingart, K.R., Flores, L.L., Dendukuri, N., Schiller, I., Laal, S., Ramsay, A., Hopewell, P. C., Pai, M., 2011. Commercial Serological tests for the diagnosis of active pulmonary and extrapulmonary tuberculosis: an updated systematic review and Meta-Analysis. *PLoS Med.* 8 <https://doi.org/10.1371/journal.pmed.1001062>.
- Tripathi, K., Driskell, J.D., 2018. Quantifying bound and active antibodies conjugated to gold nanoparticles: a comprehensive and robust approach to evaluate immobilization chemistry. *ACS Omega* 3, 8253–8259. <https://doi.org/10.1021/acsomega.8b00591>.
- Wood, A., Barizuddin, S., Darr, C.M., Mathai, C.J., Ball, A., Minch, K., Somoskovi, A., Hamasur, B., Connelly, J.T., Weigl, B., Andama, A., Cattamanchi, A., Gangopadhyay, K., Bok, S., Gangopadhyay, S., 2019. Ultrasensitive detection of lipoarabinomannan with plasmonic grating biosensors in clinical samples of HIV negative patients with tuberculosis. *PLoS One* 14, 1–12. <https://doi.org/10.1371/journal.pone.0214161>.
- Wood, R., Lawn, S.D., 2012. Challenges facing lipoarabinomannan urine antigen tests for diagnosing HIV-associated tuberculosis. *Expert Rev. Mol. Diagn.* 12, 549–551. <https://doi.org/10.1586/erm.12.52>.
- World Health Organisation, 2019. *Global Tuberculosis Report 2019*. WHO.
- Wu, W. Te, Chen, C.H., Chiang, C.Y., Chau, L.K., 2018. Effect of surface coverage of gold nanoparticles on the refractive index sensitivity in fiber-optic nanoplasmonic sensing. *Sensors* 18, 23–30. <https://doi.org/10.3390/s18061759>.
- Yalov, V.P., Troitsky, G.V., Demchenko, A.P., Generalov, I.V., 1975. Temperature and pH dependent changes of immunoglobulin G structure. *Biochim. Biophys. Acta* 386, 155–167. [https://doi.org/10.1016/0005-2795\(75\)90256-1](https://doi.org/10.1016/0005-2795(75)90256-1).